On-Wafer Electron Beam Detectors by Floating-Gate FinFET Technologies

Shi Jiun Wang, Chih-An Yang, Burn Jeng Lin, Chrong Jung Lin, and Ya-Chin King, *Senior Member, IEEE*

***Abstract*— A novel electron beam detector made on Si wafers by the advanced CMOS FinFET processes has been proposed in this study. Through electron beam (e-Beam) charging of on-wafer sensing pads, electron dosage can be registered on the detector for follow-up read-out. Without external power or battery connections, this detector has successfully delivered on-chip dosage, intensity, and energy after e-Beam exposure.**

***Index Terms*— CMOS compatible, electron beam detection, FinFET, on-wafer.**

I. Introduction

WITH the rise of IoT and wearable electronic devices, the demand for semiconductor-based products has grown rapidly, which facilitates the rapid development of semiconductor technologies in this highly competitive environment. As widely known in the semiconductor field, the pursuit of conforming to Moore's law pushed many semiconductor manufacturers toward the aggressive scaling of technology nodes. The lithography plays the most critical role in defining patterns with even smaller critical dimensions [1], [2], and it has become the key focus for the top players in the industry for maintaining their leading edge. In the lithography systems providing the critical dimensions down to nanometer regimes, short-wavelength light sources, such as EUV/DUV and electron beam (e-Beam), have become indispensable [3]–5]. To ensure stable and reliable transfer of patterns, on-site real-time detection of the electron distribution on the projected surface can be essential to reaching and maintaining a high product yield.

In the past, to obtain feedback on e-Beam intensity, conventional sensors such as charge-coupled devices (CCDs) and active pixel sensors (APSs), are commonly used [6]. CCDs utilized potential wells and/or floating nodes for collecting photo-electrons induced by photoelectric effects [7], [8]. While in APS sensor arrays, each pixel generally is composed of a photodiode and multiple transistors that limit its spatial resolutions [9]–[11].

However, there are some restrictions on using the existing solution in advanced lithography systems. To achieve high charge transfer efficiency, CCDs require specialized fabrication processes [12]–[14]. For APS arrays can be made with processes which is compatible to CMOS process, the photodiodes are not optimized for electron beam collection [15], [16].

On the other hand, for obtaining the feedback of e-Beam intensity on the projected plane, some other e-Beam detectors have been proposed such as the fiber-optic scintillating detectors and ferroelectric-crystal detectors [17], [18]. In fiber-optic scintillating detectors is composed of organic scintillator [19]–[21] and plastic optical fiber (POF) [22]–[24]. Through scintillating light generated from e-Beam exposure is transferred to photoelectric diode array by POF for final signal readout. Ferroelectric-crystal detector [25], [26] utilizes one of the ferroelectric/piezoelectric materials which generates the heat when it under the e-Beam exposure [27]. Afterward, the heat changes the crystal surface of polarization that produces the responding voltage becomes the readout signal [28].

Nevertheless, to obtain the signals from these arrays, all the above requires complex peripheral circuits and timing control, which cannot be easily integrated directly on a Si wafer. In addition, both sensing arrays can only sense e-Beam dosage in a real-time fashion which requires power connection or/or battery unit in the sensor modules [29], [30], making their installation onto e-Beam systems more complex and less flexible. In addition, under the e-Beam sensing, with the high optical resolution and high energy e-Beam is found to penetrate deep into the sensing plan, result in serious disturbance on the sensing devices, leading to unexpected damage and/or distortion of the signals.

In this work, a novel on-wafer e-Beam sensing device is proposed. This new sensor device exhibits extraordinary ability for sensing e-Beam dosage with high sensitivity and dynamic sensing range, through a floating-gate structure to enable simultaneous detecting and recoding operations. The detectors can be fabricated by standard CMOS FinFET processes, which enables the proposed sensing array to be applied to advanced technologies, which makes the adaption of the sensing module much more flexible and readily as part of the on-chip test lines.

Manuscript received April 20, 2021; revised June 1, 2021; accepted June 7, 2021. Date of publication June 22, 2021; date of current version August 23, 2021. This work was supported in part by Taiwan Semiconductor Manufacturing Company and in part by the Ministry of Science and Technology, Taiwan, under Project MOST 108-2622-8-007-017. The review of this article was arranged by Editor R. Kuroda. *(Corresponding author: Ya-Chin King.)*

Shi Jiun Wang, Chih-An Yang, Chrong Jung Lin, and Ya-Chin King are with the Institute of Electronics Engineering, National Tsing Hua University, Hsinchu 300, Taiwan (e-mail: ycking@ee.nthu.edu.tw).

Burn Jeng Lin is with the Institute of Photonics Technologies, National Tsing Hua University, Hsinchu 300, Taiwan.

Digital Object Identifier 10.1109/TED.2021.3088393

This work is licensed under a Creative Commons Attribution 4.0 License. For more information, see https://creativecommons.org/licenses/by/4.0/

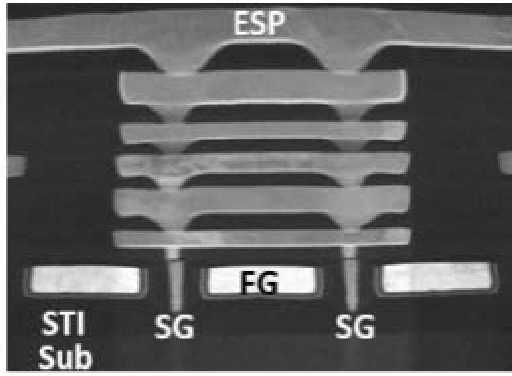

(a)

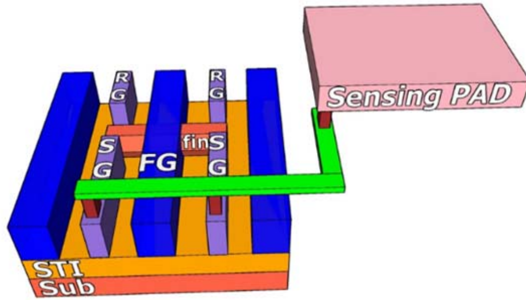

(b)

Fig. 1. (a) TEM cross-sectional view of connecting structure of FCS and ESP. The FG length is 140 nm. (b) 3-D illustration of the on-wafer e-Beam detector.

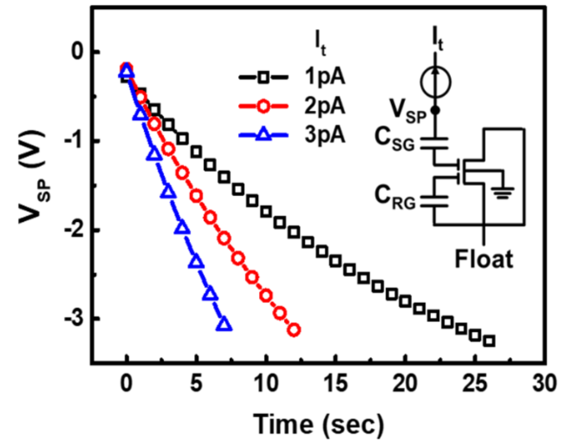

Fig. 2. With constant test current, I_t, applied, measured V_{SP} response indicates that the sensing pad capacitance is around 80 fF.

II. Device Structure and Operation Principles

The detector samples are fabricated by a 16-nm standard FinFET CMOS logic process [31], [32]. Fig. 1(a) shows the TEM cross-sectional view of connecting structure of the fin coupling structure (FCS). A 3-D schematic of the proposed on-wafer e-Beam detector which is composed of the floating gate (FG) recorder and a stacked energy-sensing pad (ESP) for sensing/collecting electrons injected by e-Beam is shown in Fig. 1(b). Similar concepts which use metal pads for sensing/collecting charge particles have been proposed in previous studies [33], [34]. To maximize the collection efficiency, the detectors employed all available metal layers from the CMOS process used for our sample fabrication, which includes nine—metal layers. For the part of the FG recorder, the sensing gate (SG), and reading gate (RG) in Fig. 1(b) are referred to as the slot contact landed on shallow trench isolation (STI) region, which between adjacent transistors is mainly for preventing interference between signals. The SG is connected to ESP to couple the ESP potential to the FG. whereas the RG is connected to another coupling structure for read operations. During e-Beam exposure, ESP is charged to a high negative potential, V_{ESP}, which is coupled to the FG, leading to the electron ejection out of FG through tunneling effect, causing a change in its storage charge, ΔQ for e-Beam dosage responding. Hence, the e-Beam intensity, which directly correlates to V_{ESP}, can be reflected by ΔQ.

For the discussion of mathematical analysis of the tunneling effect, the tunneling process for electrons can be described through the time-dependent Fowler–Nordheim (FN) tunneling mechanism, in which the current density (J_{FN}) under a specific electric field across the gate oxide (E_{ox}) can be described as follows:

$$J_{FN} = aE_{ox}^2 \exp\left(-\frac{b}{E_{ox}}\right) \quad (1)$$

where a and b are the material-related constants, including gate dielectric constant, energy barrier width, and gate work function. The equation gives that the tunneling current level which controls the rate of $\Delta Q(t)$, which in turn affects the responsivity of the detector.

Fig. 2 shows the voltage on the sensing pad when different test current, I_t, of 1, 2, 3 pA is applied. When electrons inject onto the ESP, the pad can be considered as a capacitor being charge up by the e-Beam current. The capacitance level of the sensing pad, C_{SP}, affects how fast the V_{SP} raises under a specific e-Beam intensity. Through measuring the results of V_{SP} in response to the applied test current, capacitance of the sensing pad, C_{SP}, can be extracted, which is found to be around 80 fF.

In Fig. 3, the I_D–V_{RG} characteristic curves of a detector before and after electron beam injection are compared. With an intensity of 1 μC/cm^2·s, 5-keV e-Beam energy, the threshold voltage, V_{TH}, of FG transistors are found to shift to the left. As charging of the ESP occurs, the negative V_{sp} is coupled to FG, leading to the electron ejection from the FG. Under the same intensity, increasing exposure time causes more electrons to be pushed out of FG, leading to positive ΔQ on FG, as shown in Fig. 6, which in turn resulting in a more negative V_{th} shift, see Fig. 3.

Fig. 4(a) shows the 3-D schematic of the ESP structure which is composed of nine-stacked metal layers is responsible for collecting electrons under e-Beam exposure. The cross-section illustration in Fig. 4(b) shows the relative thickness of each metal layer, provided by the standard CMOS process. The sensing pad area as well as the stacked metal layers is also revealed, where the top metal layers are much thicker than

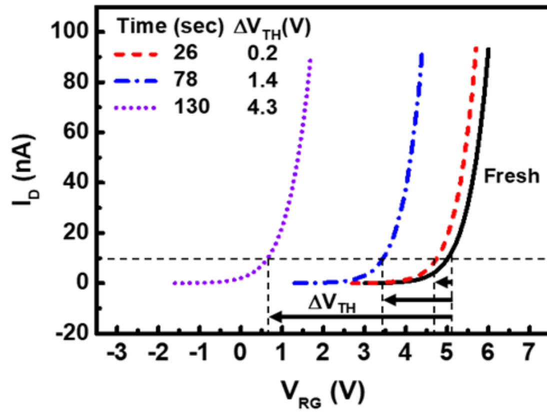

Fig. 3. I_D–V_{RG} characteristics show negative V_{TH} shift after e-Beam exposure at an intensity of 1 μC/cm^2·s, energy of 5 keV.

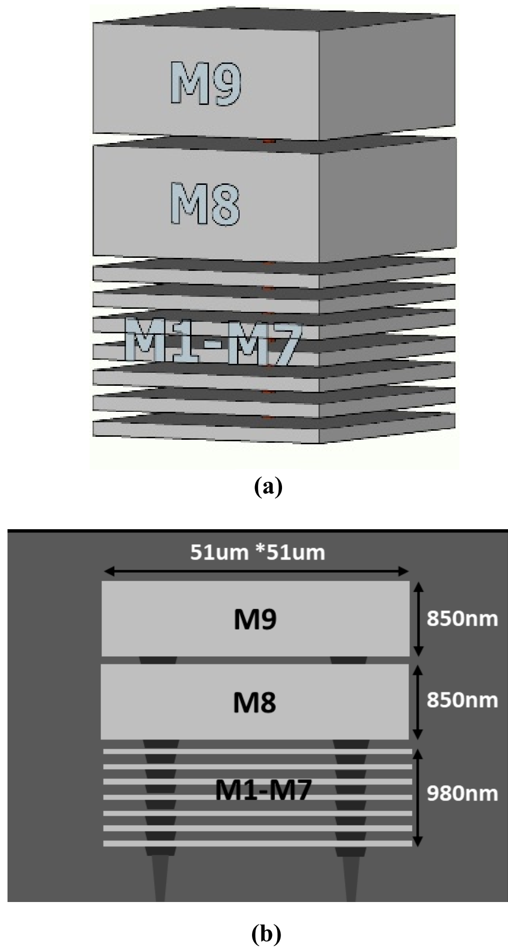

Fig. 4. (a) 3-D schematic of the collection pad structure. (b) 2-D cross-section showed the area and thicknesses of each metal layer and the spacing between.

the rest. During the whole exposure experiment, the e-Beam is focused on the ESP region of the samples only, hence, the FinFET transistors were not exposed to e-Beam injection, and hence, its characteristics remain stable.

III. Results and Discussion

Under different e-Beam energy, the experimental results in Fig. 5 compare the change in FG charge, ΔQ, defined as $Q_{\mathrm{FG.after}}-Q_{\mathrm{FG.fresh}}$, versus the overall e-Beam dosage. The results reveal that the higher the e-Beam energy, the less the change in FG charge, ΔQ. It is found that as e-Beam energy increases, the projected region deepens. When more electrons penetrate underneath the Si surface, electrons are collected by the ESP becomes less, which causes a lower V_{SP} response, in turn, less ΔQ is found after exposure. On the other hand, it is also worth noting that under the low e-Beam dosage, no observable ΔQ is found. This is because under low e-Beam intensity the potential on ESP is not enough for FN tunneling to occur, hence, there is no change in FG charge.

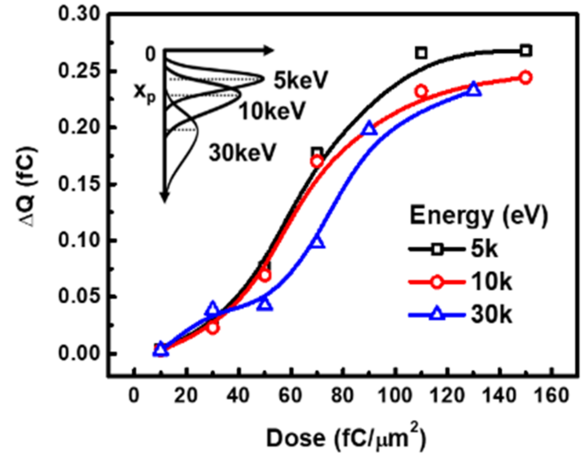

Fig. 5. Projected range deepened under surface as energy increased. With a stacked sensing pad, the response of the detector decreases as the e-Beam energy increases.

To estimate the current levels on the sensing pad, I_{SP}, in response to a certain applied e-Beam current, I_{eB}, test current is applied to the sensing pad of the detector. By matching ΔQ response versus time obtained from e-Beam experiments, the equivalent I_{SP} can be extracted. It is found that the responding I_{SP} is lower than I_{eB} applied, suggesting that not all injected electrons are collected by the ESP.

As illustrated in the inset of Fig. 5, as energy increases, the electron projection range increases. When electron penetrates beyond these metal layers into the Si substrate, the electron collection efficiency is expected to decrease. Fig. 7 shows the response for ΔQ versus exposure time under the different e-Beam energy. The electron collection efficiency, extracted from the I_{SP} found in Fig. 6, is summarized in Fig. 7. As expected, when energy increases, ESP collection efficiency, η, decreases.

The data retention characteristic of the FG transistor is shown in Fig. 8. After e-Beam exposure, the Q_{FG} stored in the FG remains relatively stable. This suggests that this recording detector can keep the signal for a long enough time, enabling follow-up measurement to be completed outside the processing chamber, independently.

Under the e-Beam exposure, it has been reported that the dangling bond formed by the high energy electron injection and the moisture absorption is known to change the dielectric properties of low-k film between metal layers [35].

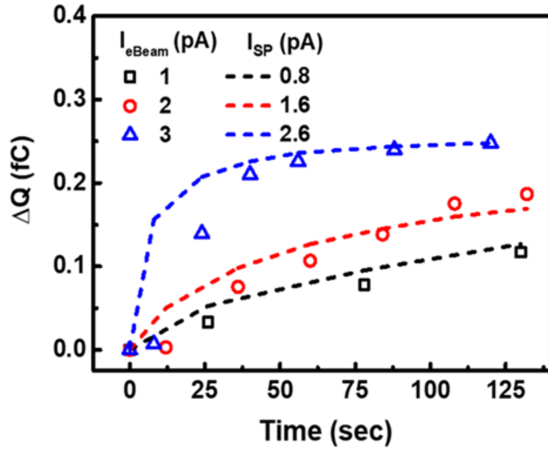

Fig. 6. Detector response under e-Beam and that by applying equivalent level of current, I_{SP}, on the sensing pad, to obtain the matching responses.

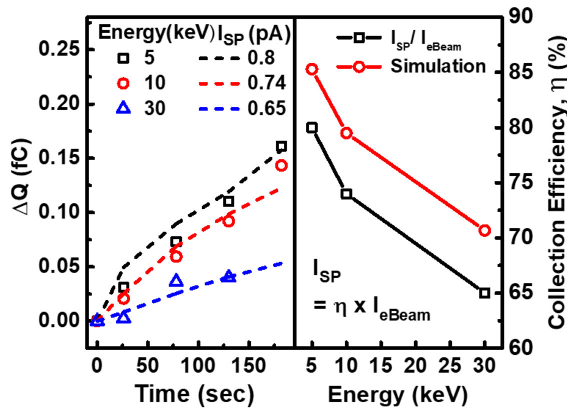

Fig. 7. Higher energy beam penetrates deeper under the surface, the e-collection efficiency, η, decreases. Measured η is slightly lower than that extracted from experiments.

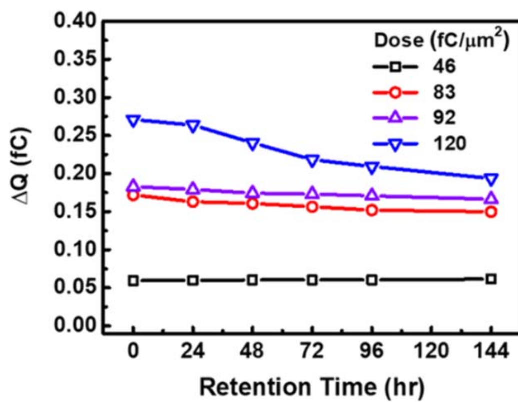

Fig. 8. Q_{FG} inside the floating gate remains relative stable after six days. While samples with higher Q_{FG} subject to some charge gain effect.

As the dielectric constant of the material between the slot contact and the metal gate changes, an undesirable effect on the readout current of the detectors may occurs. As shown in Fig. 9, the change in subthreshold I_D–V_{RG} characteristics

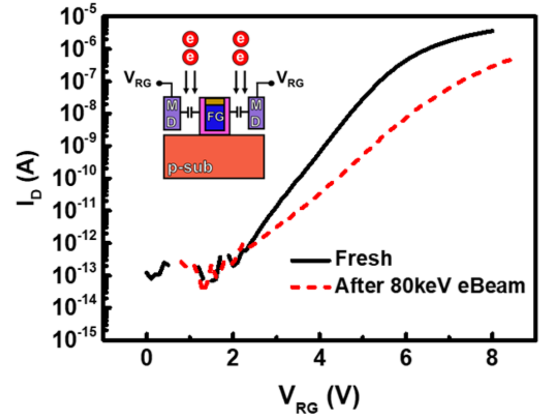

Fig. 9. Higher energy beam of 200 μC/cm^2, exposure time of 1 s, is found to cause a range in the subthreshold swing of the detectors, with lower coupling ratio.

TABLE I
COMPARISON OF DEVICE PROPERTIES

Features	CMOS Compatibility	External Power	Electrical Signal
This work	✓	✗	✓
[17]	✗	✓	✓
[18]	✗	✓	✓
[34]	✗	✓	✗
[35]	✗	✓	✗
[36]	✗	✓	✓

on the FG transistor after high energy e-Beam exposure is observed. Aside from ΔQ, the signal, these additional changes on the FG detectors can be problematic from obtaining clear signals in response to e-Beam dosage. Hence, methods of confining e-Beam distributions are necessary before we extend this new on-wafer detector to the high energy e-Beam systems.

The main novelty of this work is to deliver an on-wafers electron beam detector that can record the responses without external power or battery connections. Sensing of e-Beam dosage and intensity after exposure has been demonstrated successfully by the experimental data.

IV. CONCLUSION

In Table I, a variety of the characteristics and properties of different types of e-Beam detectors are compared. The e-Beam detector proposed in the past all needed the battery/external power and a peripheral circuit for signal readout, which lead to complexity in the incorporating of detector for in-line monitoring. While on the detection principle, some of them detect the e-Beam signal through the chemical reaction, such as the heat expansion, and light generation that will make it less compatible with the electronic control system. In contrast, the novel e-Beam detector proposed in this work features full compatibility with CMOS technology, purely electrical

response, and can operate without battery and external power supply during sensing. Therefore, the detectors provide a novel e-Beam sensing scheme for on-chip in-monitoring systems [36]–[38].

A novel FG e-Beam detector fabricated by nanoscale FinFET CMOS technology is proposed. Coupled by a stack-metal ESP, the FG of the readout transistor can successfully record e-Beam dosage as ESP is charged by the injected electrons. This power-free and on-wafer e-Beam detector can be used in line detection and offer timely feedback for the advanced lithography system.

References

[1] G. E. Moore, "Cramming more components onto integrated circuits, reprinted from electronics, volume 38, number 8, April 19, 1965, pp. 114 ff," *IEEE Solid-State Circuits Soc. Newslett.*, vol. 11, no. 3, pp. 33–35, Sep. 2006, doi: 10.1109/N-SSC.2006.4785860.

[2] E. Mollick, "Establishing Moore's law," *IEEE Ann. Hist. Comput.*, vol. 28, no. 3, pp. 62–75, Jul. 2006, doi: 10.1109/MAHC.2006.45.

[3] B. Kneer, S. Migura, W. Kaiser, J. T. Neumann, and J. van Schoot, "EUV lithography optics for sub-9 nm resolution," *Proc. SPIE*, vol. 9422, pp. 1–10, Mar. 2015, doi: 10.1117/12.2175488.

[4] C. W. Gwyn, R. Stulen, D. Sweeney, and D. Attwood, "Extreme ultraviolet lithography," *J. Vac. Sci. Technol. B, Microelectron.*, vol. 16, no. 6, pp. 3142–3149, Dec. 1998, doi: 10.1116/1.590453.

[5] A. A. Tseng, K. Chen, C. D. Chen, and K. J. Ma, "Electron beam lithography in nanoscale fabrication: Recent development," *IEEE Trans. Electron. Packag. Manuf.*, vol. 26, no. 2, pp. 141–149, Apr. 2003, doi: 10.1109/TEPM.2003.817714.

[6] A. R. Faruqi, R. Henderson, M. Pryddetch, P. Allport, and A. Evans, "Direct single electron detection with a CMOS detector for electron microscopy," *Nucl. Instrum. Methods Phys. Res. A, Accel. Spectrom. Detect. Assoc. Equip.*, vol. 546, nos. 1–2, pp. 170–175, Jul. 2005, doi: 10.1016/j.nima.2005.03.023.

[7] M. P. Benk *et al.*, "Demonstration of 22-nm half pitch resolution on the SHARP EUV microscope," *J. Vac. Sci. Technol. B, Microelectron.*, vol. 33, no. 6, Nov. 2015, Art. no. 06FE01, doi: 10.1116/1.4929509.

[8] W. S. Boyle and G. E. Smith, "Charge coupled semiconductor devices," *Bell Syst. Tech. J.*, vol. 49, no. 4, pp. 587–593, Apr. 1970, doi: 10.1002/j.1538-7305.1970.tb01790.x.

[9] A. Dickinson, B. Ackland, E.-S. Eid, D. Inglis, and E. R. Fossum, "Standard CMOS active pixel image sensors for multimedia applications," in *Proc. 16th Conf. Adv. Res. VLSI*, Chapel Hill, NC, USA, 1995, pp. 214–224, doi: 10.1109/ARVLSI.1995.515622.

[10] K. S. Karim, F. Taghibakhsh, M. H. Izadi, N. Safavian, and D. Wu, "Current mode active pixel sensor architectures for large area digital imaging," in *Proc. Int. Conf. Microelectron.*, Sharjah, United Arab Emirates, Dec. 2008, pp. 433–436, doi: 10.1109/ICM.2008.5393796.

[11] R. E. Coath *et al.*, "A low noise pixel architecture for scientific CMOS monolithic active pixel sensors," *IEEE Trans. Nucl. Sci.*, vol. 57, no. 5, pp. 2490–2496, Oct. 2010, doi: 10.1109/TNS.2010.2052469.

[12] P. Touron, F. Roy, P. Magnan, O. Marcelot, S. Demiguel, and C. Virmontois, "Capacitive trench-based charge transfer device," *IEEE Electron Device Lett.*, vol. 41, no. 9, pp. 1388–1391, Sep. 2020, doi: 10.1109/LED.2020.3014431.

[13] M. LeNoble, J. V. Cresswell, and R. R. Johnson, "A two-phase GaAs cermet gate charge-coupled device," *IEEE Trans. Electron Devices*, vol. 37, no. 8, pp. 1796–1799, Aug. 1990, doi: 10.1109/16.57128.

[14] K. Hatano *et al.*, "A two-phase CCD register with charge injected floating gate electrodes," *IEDM Tech. Dig.*, San Francisco, CA, USA, Dec. 1996, pp. 903–906, doi: 10.1109/IEDM.1996.554125.

[15] S.-H. Jo, M. Bae, J. Jung, and J.-K. Shin, "CMOS active pixel sensor with variable dynamic range using a double-photodiode feedback structure," in *Proc. IEEE Int. Instrum. Meas. Technol. Conf.*, Binjiang, China, May 2011, pp. 1–4, doi: 10.1109/IMTC.2011.5944353.

[16] S. Tedde, E. S. Zaus, J. Furst, D. Henseler, and P. Lugli, "Active pixel concept combined with organic photodiode for imaging devices," *IEEE Electron Device Lett.*, vol. 28, no. 10, pp. 893–895, Oct. 2007, doi: 10.1109/LED.2007.905425.

[17] A.-S. Beddar and P. D. Higgins, "Use of ferroelectric-crystal detectors for electron dosimetry," *IEEE Trans. Ultrason., Ferroelectr., Freq. Control*, vol. 37, no. 1, pp. 26–29, Jan. 1990, doi: 10.1109/58.46966.

[18] B. Lee *et al.*, "Characterization of one-dimensional fiber-optic scintillating detectors for electron-beam therapy dosimetry," *IEEE Trans. Nucl. Sci.*, vol. 55, no. 5, pp. 2627–2631, Oct. 2008, doi: 10.1109/TNS.2008.2002578.

[19] D. L. Chichester, S. M. Watson, and J. T. Johnson, "Comparison of BCF-10, BCF-12, and BCF-20 scintillating fibers for use in a 1-dimensional linear sensor," *IEEE Trans. Nucl. Sci.*, vol. 60, no. 5, pp. 4015–4021, Oct. 2013, doi: 10.1109/TNS.2013.2277799.

[20] V. Turgeon, G. Kertzscher, L. Carroll, R. Hopewell, G. Massarweh, and S. A. Enger, "Characterization of scintillating fibers for use as positron detector in positron emission tomography," *Phys. Medica*, vol. 65, pp. 114–120, Sep. 2019, doi: 10.1016/j.ejmp.2019.08.009.

[21] S. G. Novikov *et al.*, "Simulating a scintillation fiber detector of the activities of ionizing radiation sources," *Results Phys.*, vol. 6, pp. 16–17, Dec. 2016, doi: 10.1016/j.rinp.2015.12.002.

[22] A.-M. Frelin *et al.*, "Spectral discrimination of Čerenkov radiation in scintillating dosimeters," *Med. Phys.*, vol. 32, no. 9, pp. 3000–3006, Sep. 2005, doi: 10.1118/1.2008487.

[23] T. O. White, "Scintillating fibers," *Nucl. Instrum. Methods Phys. Res. A, Accel. Spectrom. Detect. Assoc. Equip.*, vol. 273, pp. 820–825, Dec. 1988, doi: 10.1016/0168-9002(88)90102-7.

[24] A. S. Beddar, "Plastic scintillation dosimetry and its application to radiotherapy," *Radiat. Meas.*, vol. 41, pp. S124–S133, Dec. 2006, doi: 10.1016/j.radmeas.2007.01.002.

[25] S. Mascarenhas, H. Vargas, and C. L. Cesar, "A photoacoustical radiation dosimeter," *Med. Phys.*, vol. 11, no. 1, pp. 73–74, Jan. 1984, doi: 10.1118/1.595456.

[26] M. H. de Paula, A. A. Carvalho, S. Mascarenhas, and R. L. Zimmerman, "A new radiation dosimeter using a pyroelectric detector," *Med. Phys.*, vol. 11, no. 6, pp. 866–868, Nov. 1984, doi: 10.1118/1.595587.

[27] F. Kulcsar, "Electromechanical properties of lead titanate zirconate ceramics modified with certain three-or five-valent additions," *J. Amer. Ceram. Soc.*, vol. 42, no. 7, pp. 343–349, Jul. 1959, doi: 10.1111/j.1151-2916.1959.tb14321.x.

[28] B. Jaffe, R. S. Roth, and S. Marzullo, "Piezoelectric properties of lead zirconate-lead titanate solid-solution ceramics," *J. Appl. Phys.*, vol. 25, no. 6, pp. 809–810, Jun. 1954, doi: 10.1063/1.1721741.

[29] J.-K. Li *et al.*, "Self-driven visible-blind photodetector based on ferroelectric perovskite oxides," *Appl. Phys. Lett.*, vol. 110, no. 14, Apr. 2017, Art. no. 142901, doi: 10.1063/1.4979587.

[30] C. H. Park, A. Lee, R. Kim, and J. H. Moon, "Evaluation of the detection efficiency of LYSO scintillator in the fiber-optic radiation sensor," *Sci. Technol. Nucl. Installations*, vol. 2014, Apr. 2014, Art. no. 248403, doi: 10.1155/2014/248403.

[31] M. Jurczak, N. Collaert, A. Veloso, T. Hoffmann, and S. Biesemans, "Review of FINFET technology," in *Proc. IEEE Int. SOI Conf.*, Foster City, CA, USA, Oct. 2009, pp. 1–4, doi: 10.1109/SOI.2009.5318794.

[32] A. Kaneko *et al.*, "Sidewall transfer process and selective gate sidewall spacer formation technology for sub-15 nm FinFET with elevated source/drain extension," in *IEDM Tech. Dig.*, Washington, DC, USA, Dec. 2005, pp. 844–847, doi: 10.1109/IEDM.2005.1609488.

[33] I. Takayanagi, J. Nakamura, E. R. Fossum, K. Nagashima, T. Kunihoro, and H. Yurimoto, "Dark current reduction in stacked-type CMOS-APS for charged particle imaging," *IEEE Trans. Electron Devices*, vol. 50, no. 1, pp. 70–76, Jan. 2003, doi: 10.1109/TED.2002.806963.

[34] S. Fuerstenau, G. Soli, T. Cunningham, B. Hancock, B. Pain, and M. Sinha, "Active pixel sensors for mass spectrometry," *Int. J. Mass Spectrometry*, vol. 215, nos. 1–3, pp. 101–111, Apr. 2002, doi: 10.1016/S1387-3806(01)00589-9.

[35] T. C. Chang, T. M. Tsai, P. T. Liu, C. W. Chen, and T. Y. Tseng, "Study on the effect of electron beam curing on low-K porous organosilicate glass (OSG) material," *Thin Solid Films*, vols. 469–470, pp. 383–387, Dec. 2004, doi: 10.1016/j.tsf.2004.08.178.

[36] H. J. Hyun *et al.*, "Electron beam test results with a DC-coupled single-sided strip detector," in *Proc. IEEE Nucl. Sci. Symp. Conf. Rec.*, Honolulu, HI, USA, Oct. 2007, pp. 642–644, doi: 10.1109/NSSMIC.2007.4436414.

[37] R. Chechik, A. Breskin, I. Frumkin, A. Gabriel, and M. Kocsis, "Real-time secondary electron emission detector for high-rate X-ray crystallography," *IEEE Trans. Nucl. Sci.*, vol. 43, no. 3, pp. 1248–1252, Jun. 1996, doi: 10.1109/23.506672.

[38] D. M. Shu, P. K. Job, T. M. Kuzay, and S. Korenev, "CVD-diamond-based position-sensitive detector test with electron beam from a Rhodotron/sup TM/ accelerator," in *Proc. Part. Accel. Conf.*, Chicago, IL, USA, vol. 3, Jun. 2001, pp. 2435–2437, doi: 10.1109/PAC.2001.987408.